Title: Deciphering the role of evapotranspiration in declining relative humidity trends over land

Authors: Yeonuk Kim,[1]* Mark S. Johnson,[1,2]

Affiliations

[1] Institute for Resources, Environment and Sustainability, University of British Columbia, Vancouver, BC, Canada

[2] Department of Earth, Ocean and Atmospheric Sciences, University of British Columbia, Vancouver, BC, Canada

* Correspondence to: Yeonuk Kim (yeonuk.kim@ubc.ca)

Abstract

In recent decades, relative humidity over land (RH_L) has declined, driving increases in droughts and wildfires. Previous explanations attribute this trend to insufficient moisture advection from the ocean to sustain RH_L, but this ignores atmospheric moisture supplied from terrestrial evapotranspiration (E_L). Importantly, current state-of-the-art climate models underestimate the observed RH_L trend, and the cause is not fully understood. Here, we show that relative changes in humidity over land, unaccounted for by ocean advection, are quantitatively equivalent to relative changes in E_L on a global scale. This finding is consistent across climate models and climate reanalysis datasets, despite discrepancies in E_L trends among them. Differences in E_L trends are identified as the primary cause of the RH_L bias expressed in climate models. These results suggest that current climate models may overestimate E_L intensifications, leading to an underestimation of land-atmosphere drying, with significant implications for accurately predicting droughts, wildfires, and climate adaptation.

MAIN TEXT

Human-induced climate change is expected to have significant impacts on Earth's water cycle[1]. Reliable predictions of future water resources require a comprehensive understanding of how climate change affects land evapotranspiration (E_L)[2-4], which represents the sum of evaporation from soil, intercepted water, and plant transpiration. While many studies have investigated the effects of climate change on actual E_L, the complex interactions between the atmosphere, land surface, soil moisture, and vegetation make it challenging to accurately predict changes in E_L. There are few long-term observational records of E_L, forcing a reliance on indirect methods to determine E_L trends at global and decadal scales. Our understanding of changes in E_L remains limited, exemplified by a substantial uncertainty in its estimated long-term changes[5,6] and a prolonged scientific debate about the impact of warmer and drier atmospheric conditions on future changes in E_L[7-14].

The complexity of discerning the influence of anthropogenic climate change on E_L is further complicated by the reciprocal relationship between E_L and the atmospheric state. Atmospheric conditions not only serve as drivers of E_L but also are influenced by E_L, given that E_L acts as a significant moisture source to the air, particularly in inland regions[15-20]. Consequently, the uncertainty in E_L predictions has been identified as a significant contributor to uncertainty in atmospheric state predictions[21,22]. Paradoxically, however, the impacts of E_L on the near-surface atmosphere are frequently overlooked under the prevailing assumption that the atmospheric state acts primarily as a demand-side driver of E_L[8].

Near-surface atmospheric observations in recent decades demonstrate an emergent decline in relative humidity over land (RH_L)[23,24]. This decline in observed RH_L is commonly explained using an ocean-influence theory[25-27]. This theory suggests that the amplified land warming compared to ocean warming is the primary cause of the RH_L decline since moisture advection from the ocean to the land is insufficient to maintain RH_L relative to increasing land surface temperatures. Consequently, warmer and drier atmospheric conditions over land are widely considered to drive a rapid increase in the atmospheric evaporative demand that could intensify E_L[7]. However, this perspective ignores the reciprocal influences of E_L and the atmospheric state[28-30]. For example, recent studies suggest that soil moisture constrains moisture supplied to the air through E_L, and this E-influenced process is crucial to represent changes in RH_L over land in climate simulations[31,32].

Therefore, it is essential to theoretically harmonize the influences on the atmospheric moisture budget over land resulting from (i) E_L and (ii) advected moisture from the ocean. This is particularly important as state-of-the-art climate models currently underestimate the well-established RH_L decline trend[33-35]. However, the fundamental reason for this bias remains unclear[36]. More importantly, this RH bias in climate models implies an underestimation of future drying and warming trends in model projections[37]. Therefore, a nuanced understanding of the influences of E_L on near-surface humidity trends over land is essential for accurately projecting future atmospheric conditions, water availability, and impacts of anthropogenic climate change on future droughts and wildfires.

Here, we aim to harmonize the influence of terrestrial E_L with the ocean-influence theory to more completely represent RH_L within an analytical framework. To this end, we first introduce a simple analytical equation explaining the relationship between changes in specific humidity and E_L from a parsimonious boundary layer moisture budget, and evaluate the proposed equation using in-situ E_L observations from the FLUXNET2015 dataset[38]. We then integrate this equation representing the emerging E-influence theory with the ocean-influence theory. Using the ERA5[39] and JRA-3Q[40] reanalysis datasets and 27 general circulation models (GCMs) contained in the Coupled Model Intercomparison Project Phase 6 (CMIP6)[41], we evaluate this integrated framework. In this way, we are able to analyze the physical constraints of changes in E_L and explain why CMIP6 climate models underestimate the emergent RH_L decline present in observations and reanalysis datasets.

***E*-influence theory**

We begin by empirically assessing divergent theories regarding water vapor sources over land. On the one hand, it has been widely hypothesized that horizontal advection from the ocean is the primary source of water vapor over land[7], forming the theoretical foundation of the ocean-influence theory[25,26]. However, other studies emphasize a dominant role for E_L as a moisture source to the air, especially for inland regions[16,42,43].

We explore these conflicting hypotheses by examining the spatial variability of specific humidity (q, kg kg^{-1}) as a function of distance from the ocean (Fig. 1). On average, the ratio of specific humidity over land (q_L) to specific humidity over the ocean (q_O) decreases rapidly from the coast to ~250 km inland, stabilizing thereafter for areas further inland. This finding that q_L is closer to q_O for areas closer to the coast suggests that horizontal advection from the ocean may be a significant source of water vapor for areas located up to 250 km inland (constituting approximately 40% of the total land area, Fig. 1). However, horizontal advection of q_O appears to become relatively negligible for areas located further inland (i.e., > 250 km), where small horizontal gradients in q_L/q_O suggest that specific humidity in inland regions could be more significantly influenced by E_L. In fact, we find that q_L/q_O is nearly constant (i.e., $\frac{d}{dx}(\frac{q_L}{q_O}) \approx 0$) for areas located between 250 km and 1000 km from a coast, which represents another 40% of the total land area. Further declines in q_L/q_O for areas >1000 km inland imply increasing moisture limitations typical of arid regions.

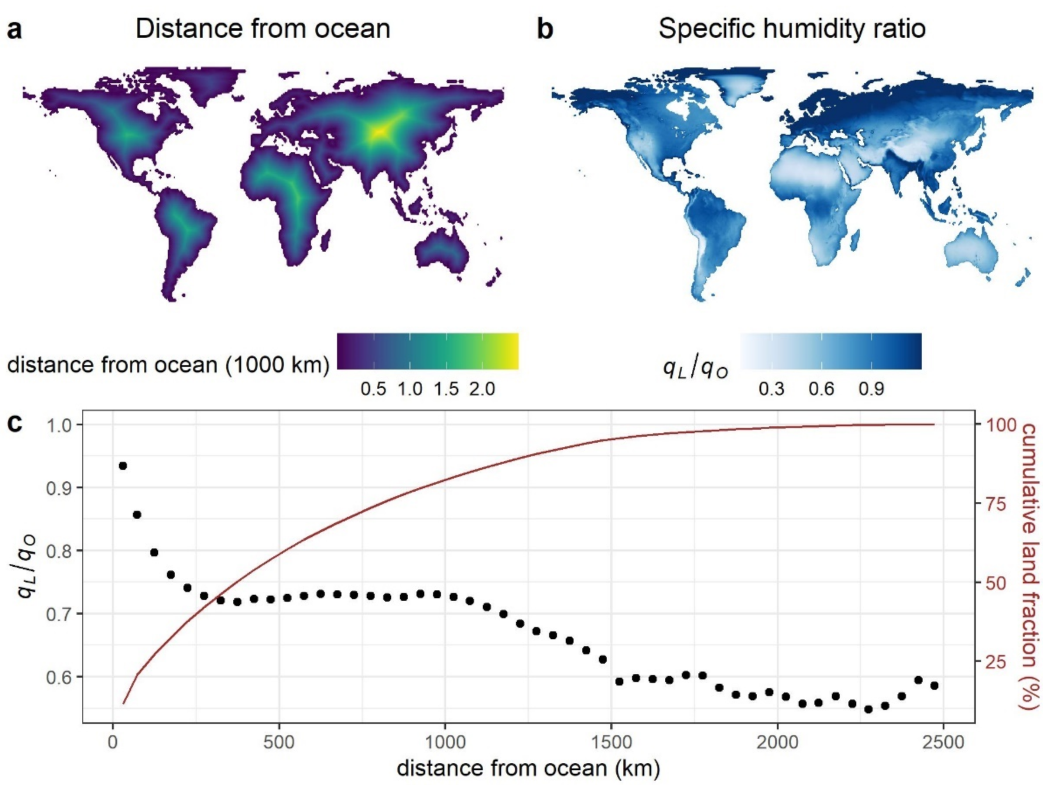

Fig. 1. Mean specific humidity ratio between land and ocean plotted against the distance from ocean. (**a**) Global map indicating the distance from ocean. (**b**) Global map of the mean specific humidity ratio between land (q_L) and ocean (q_O) in the ERA5 reanalysis over the period 1973-2022. The time-averaged q_L is calculated for each grid, while the time-averaged q_O is determined as the zonal mean at that latitude to represent the neighboring ocean. (**c**) Relationship between q_L/q_O and the distance from ocean. The black dot represents the mean q_L/q_O, calculated for binned distances from the ocean (each bin has 50 km). The cumulative land fraction (brown line) is included as a reference.

The empirical, emergent characteristics of $\frac{d}{dx}\left(\frac{q_L}{q_O}\right)$ in Fig. 1 prompts a reexamination of the derivation of the ocean-influence theory, given that horizontal advection (driven by horizontal q gradients) doesn't always emerge as the predominant moisture source, particularly over inland regions. Byrne and O'Gorman [26] proposed a parsimonious steady-state moisture budget for a boundary layer box over land (Fig. S1), which assumes negligible E in order to derive a simple moisture constraint, as expressed by Eq. 1:

$$\frac{\Delta q_L}{q_L} = \frac{\Delta q_O}{q_O} \tag{1}$$

where Δ indicates the temporal change between two periods. Eq. 1 is a summary of the ocean-influence theory, which was introduced to explain the observed decline in RH_L using the ocean advection [25-27]. The derivation of Eq. 1 involved assumptions of constant values for horizontal and vertical mixing velocities, boundary layer heights, and the specific humidity jump rate at the top of the boundary layer.

To maintain compatibility with this theoretical framework, we adopt the same moisture budget equation and assumptions for Eq. 1 while considering horizontal advection as negligible, focusing instead on the influence of E_L. In this scenario, the changes in specific humidity over land can be expressed as follows (for detailed derivation, refer to Materials and Methods):

$$\frac{\Delta q_L}{q_L} = \frac{\Delta E_L}{E_L} \tag{2}$$

Eq. 2 is the proposed theoretical constraint for changes in q_L and E_L when horizontal moisture advection is negligible and thus q_L is predominantly controlled by E_L. By rearranging Eq. 2 for ΔE_L and partitioning Δq_L into relative humidity and temperature components, we can write as follows.

$$\Delta E_L = E_L \frac{\Delta q_L}{q_L}$$

$$= E_L\left(\frac{\Delta RH_L}{RH_L} + \alpha \Delta T_L\right) \tag{3}$$

where $RH_L(= \frac{q_L}{q^*(T_L)})$ is the near-surface relative humidity over land, $q^*(T_L)$ is saturation specific humidity at the near-surface air temperature (T_L), $\alpha(= \frac{s}{q^*(T)})$ is the sensitivity of saturation specific humidity to temperature, and $s(= \frac{dq^*}{dT})$ is the linearized saturation specific humidity slope versus temperature. Here, we approximate relative humidity using specific humidity instead of water vapor pressure and linearize the Clausius-Clapeyron relationship.

Eq. 3 implies that one can simply determine ΔE_L only using atmospheric observations. However, while Eq. 1 has undergone evaluation in several prior studies[25-27,44], the viability of the proposed Eq. 3 demands a comprehensive assessment. Evaluating the proposed theory represented by Eq. 3 presents a challenge due to the absence of reliable long-term ΔE_L observations, particularly at global scale, given that E_L is more challenging to observe than specific humidity.

Alternatively, we assessed the feasibility of Eq. 3 using observed seasonal changes in ΔE_L at the field scale (e.g., a few square kilometers). We used FLUXNET2015 monthly-scale E_L and meteorological observations from 170 sites worldwide[38]. We estimated ΔE_L from Eq. 3 using monthly differences in RH_L and T_L. Subsequently, we compared observed values for ΔE_L with those estimated for ΔE_L using Eq. 3. We find that Eq. 3 effectively estimates the observed ΔE_L, particularly in inland regions (Fig. 2). The majority of inland sites (> 250 km from the ocean) exhibit a high correlation coefficient (R) between observed ΔE_L and its estimation using Eq. 3, with regression slopes close to one. On the other hand, the correlation between ΔE_L and its estimation form Eq. 3 is lower for several sites located closer to a coast (<= 250 km from ocean). These field-scale results support the viability of Eq. 3, especially in inland regions where horizontal moisture advection from the ocean becomes increasingly negligible for increasing distance from the coast. It is worth noting that the robustness of this result persisted when substituting the E_L observations with the energy balance-corrected version of E_L (see Fig. S2).

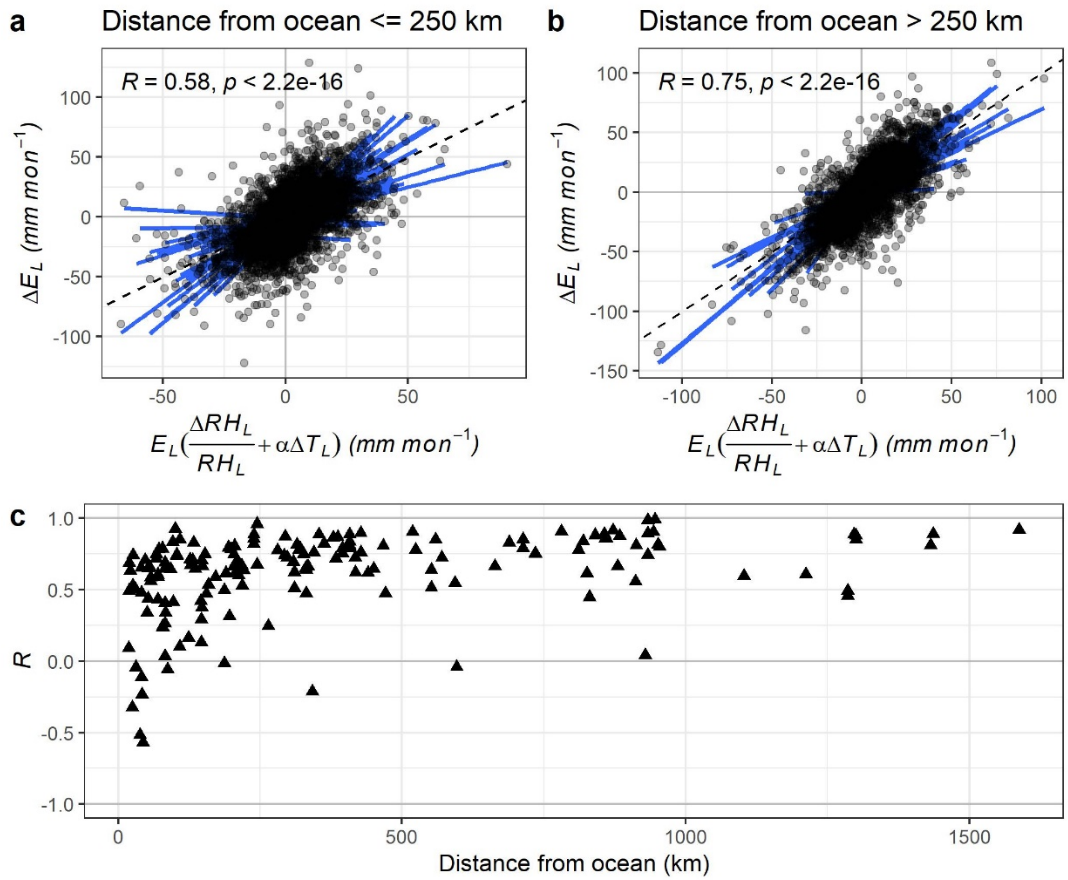

Fig. 2. Evaluation of Eq. 3 at regional scale using FLUXNET2015 dataset. Scatter plot depicting ΔE_L and its estimation using Eq. 3 for (**a**) pericoastal sites (distance from the ocean ≤ 250 km) and (**b**) inland sites (distance from the ocean > 250 km). Blue lines represent linear regression lines for each site, and black dashed lines indicate one-on-one lines. (**c**) Correlation (R) between ΔE_L and $E_L(\frac{\Delta RH_L}{RH_L} + \alpha\Delta T_L)$ for each site (y-axis) versus the distance from the ocean for each site (x-axis).

While the evaluation at field and seasonal scales supports Eq. 3, it is important to note that the direct applicability of Eq. 3 for inferring long-term changes in global E_L remains to be established. We also note that the omission of horizontal advection from the ocean in the derivation of Eq. 3 is unrealistic on a global scale, necessitating an additional line of inquiry. To further assess the performance of Eq. 3 at the global level, we employed modeled ΔE_L and atmospheric state from two latest generation reanalysis datasets and from climate simulations, assuming that ΔE_L and atmospheric state in each climate model represent internally consistent representations of the land-atmosphere-ocean coupled system [14]. Specifically, we focus on non-Polar regions located 66.5°S to 66.5°N in order to exclude the Artic and Antarctica since the ocean-influence theory is better justified at lower latitudes[27].

Our analysis revealed that Eq. 3 consistently overestimates global land ΔE_L for the recent 43 years (1980-2022) in ERA5 and JRA-3Q reanalysis datasets (Fig. 3), as well as for all 27 GCMs in CMIP6 (Fig. 4). This suggests a systematic bias in Eq. 3 on the global scale, despite its reasonable performance at regional and seasonal scales. At the regional scale, horizontal moisture advection can be both positive and negative, depending on the dryness of nearby regions, but horizontal advection from ocean to land is always positive at the global scale as q_O is always greater than q_L. Therefore, Δq_L not only increases due to the rise in E_L, but also increases due to heightened ocean advection that is driven by the increasing q_O in a warming climate. Consequently, the simplifying assumptions of Eq. 3 lead to overestimation of global-scale changes in E_L, suggesting that an additional term is needed to represent the influence of ocean advection. We now turn our attention to incorporating ocean advection into Eq. 3.

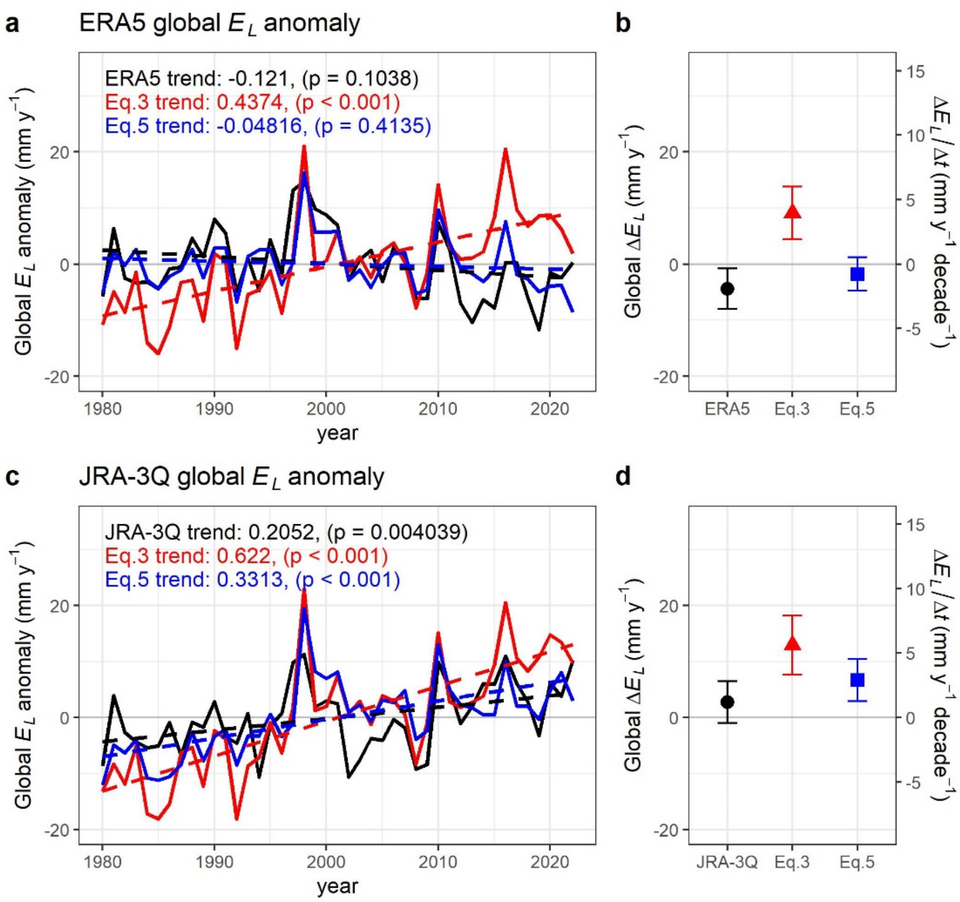

Fig. 3. Evaluation of Eq. 3 and Eq. 5 at global scale relative to ERA5 and JRA-3Q reanalysis datasets. (**a**) Global land E_L anomaly from ERA5 reanalysis (black), Eq. 3 (red), and Eq. 5 (blue) over the period 1980-2022. Dashed lines represent linear trends. (**b**) Global ΔE_L from ERA5 reanalysis (black), Eq. 3 (red), and Eq. 5 (blue), calculated as the difference between current (2003-2022) and past climate (1980-1999). Error bars represent the 95% confidence intervals, and the secondary y-axis shows the average rate of change. (**c**) Similar to panel (a) but using JRA-3Q reanalysis. (**d**) Similar to panel (b) but using JRA-3Q reanalysis. In this figure, Eqs. 3 and 5 are calculated using atmospheric variable from each reanalysis, and the artic (>66.5°N) and antarctica (<66.5°S) are masked.

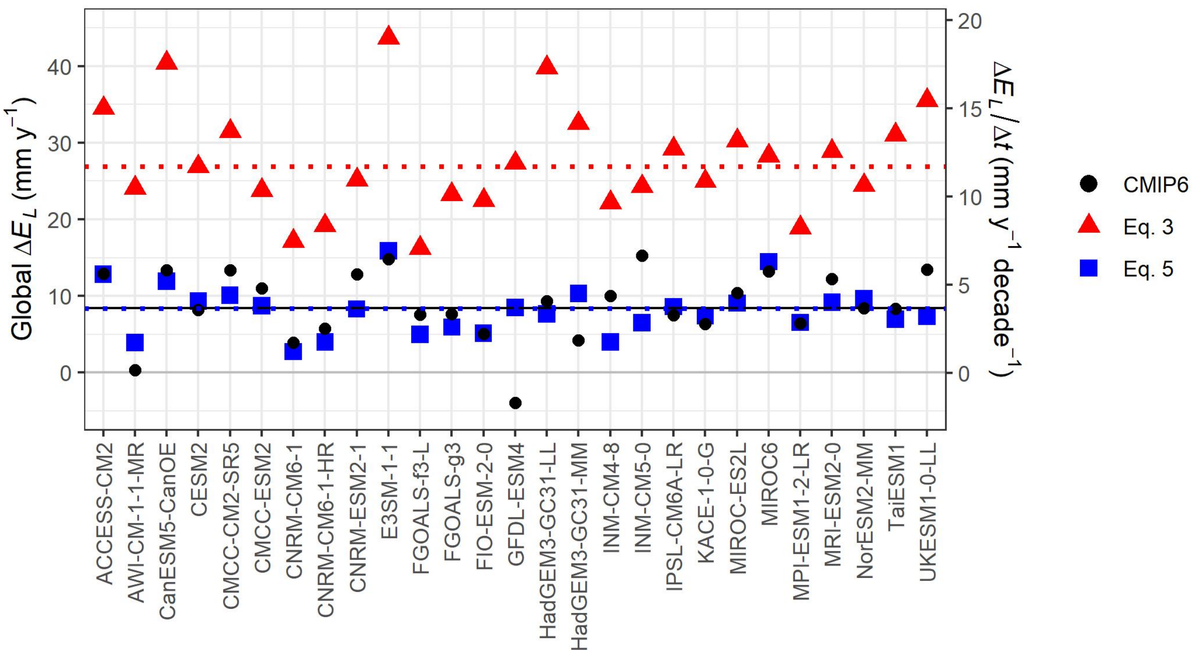

Fig. 4. Evaluation of Eq. 3 and Eq. 5 at global scale using CMIP6 climate models. Global *ΔE_L* from each climate model (black), Eq. 3 (red), and Eq. 5 (blue), calculated as the difference between current (2003-2022) and past climate (1980-1999). Dotted lines indicate median of Eq. 3 (red) and Eq. 5 (blue) while the black solid line indicates median of CMIP6. In this figure, polar regions (>66.5°N and <66.5°S) are masked.

Reintroducing ocean advection

Our analysis, illustrated in Figs. 3 and 4, indicates that Eq. 3 consistently overestimates long-term changes in E_L on a global scale, across all examined climate models and reanalysis datasets. We propose that this overestimation may be attributed to the horizontal advection of moisture from the ocean, considering that a portion of the change in q_L can be attributable to ΔE_L, while another portion results from oceanic advection. To account for the impact of ocean advection within this simple scaling framework, we account for the component of Δq_L that can be attributed to ocean advection. This adjustment is based on the ocean-influence theory (i.e., Eq. 1), as follows:

$$\Delta E_L = E_L\left(\frac{\Delta q_L}{q_L} - \gamma \frac{\Delta q_O}{q_O}\right)$$

$$\approx E_L\left(\frac{\Delta RH_L}{RH_L} + \alpha \Delta T_L - \gamma \alpha \Delta T_O\right) \quad (4)$$

where γ is a parameter introduced in our study to refine the ocean-influence theory, and T_O is near-surface air temperature over the ocean. Here, we decompose Δq into relative humidity and temperature components similar to Eq. 3 by assuming a time-constant RH over ocean[45,46].

In this simple scaling, the ocean advection is embedded in the last term of the right-hand side of Eq. 4. The introduction of γ aims to account for potential discrepancies that might arise when Eq. 1 is applied to scenarios where moisture from E_L significantly contributes to Δq_L, an aspect not explicitly covered in the original derivation of the ocean-influence theory. If Eq. 1, even within our theoretical framework, accurately depicts the ocean advection impact, then γ will be set to unity. Using CMIP6 GCMs along with ERA5 and JRA-3Q reanalysis data, we have determined that γ approximates unity on a global scale (Fig. 5), reinforcing the applicability of the ocean-influence theory within our scaling. Consequently, we adopt γ as unity, leading to the following refined equation:

$$\Delta E_L \approx E_L\left(\frac{\Delta RH_L}{RH_L} + \alpha \Delta T_L - \alpha \Delta T_O\right) \tag{5}$$

Equation 5 serves as our proposed model to estimate the long-term trend of E_L on a global scale using atmospheric variables and accounting for ocean advection. Consistent with the previous section, we apply Eq. 5 to ERA5 and JRA-3Q reanalysis data and CMIP6 GCMs. Our results show that Eq. 5 effectively reproduces the direct ΔE_L output from reanalysis (Fig. 3). Furthermore, not only does it capture the long-term ΔE_L, but Eq. 5 also reasonably replicates the interannual variability of global land E_L, particularly in the ERA5 climate reanalysis dataset (R=0.69). Also, ΔE_L estimations using Eq. 5 exhibit a much closer match with the direct ΔE_L output from CMIP6 GCMs compared to Eq. 3 (Fig. 4).

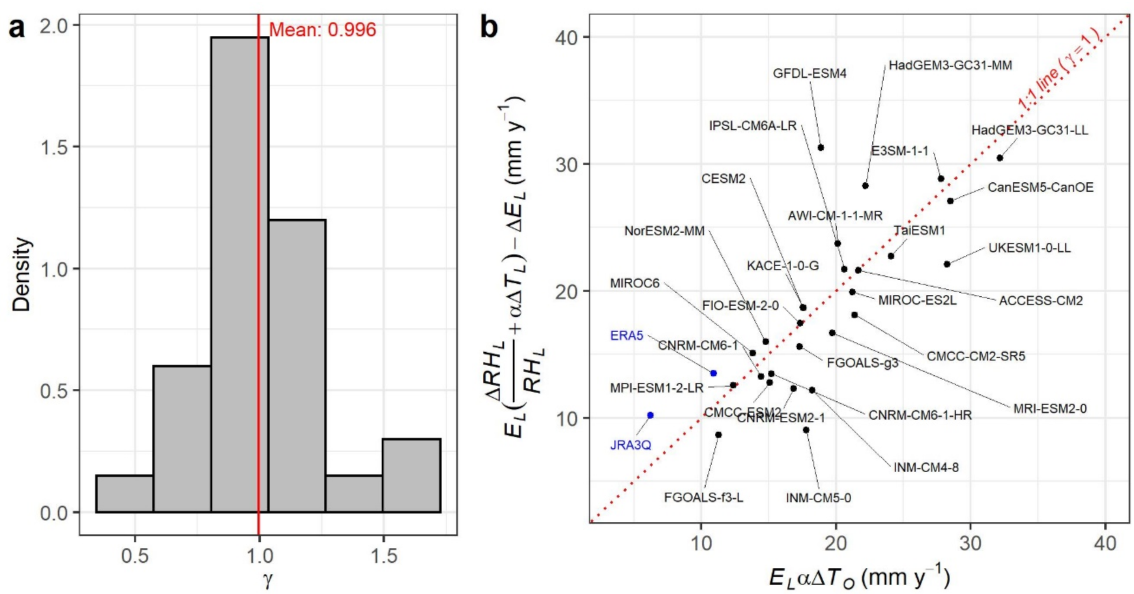

Fig. 5. Evaluation of Parameter γ. Panel (a) displays a histogram with the mean value of γ from CMIP6 GCMs and ERA5, JRA-3Q reanalysis datasets. Panel (b) offers a one-to-one plot between $E_L\left(\frac{\Delta RH_L}{RH_L} + \alpha\Delta T_L\right) - \Delta E_L$ and $E_L \alpha \Delta T_O$ for individual CMIP6 models (black dots) and reanalysis datasets (blue dots). Alignment with the one-to-one line indicates γ's approximation to unity, validating our approach to adopt γ as unity for simplifying the scaling equation. In this figure, polar regions (>66.5°N and <66.5°S) are masked to determine γ since the ocean-influence theory is better justified at lower latitudes[27].

Why do CMIP6 models underestimate the observed decline in *RH_L*?

To gain a deeper insight into the drivers behind RH_L decline in recent decades, we reorganize the proposed theory (Eq. 5) and the ocean-influence theory (Eq. 1) as follows:

$$\Delta RH_L = RH_L\Big(\overbrace{\underbrace{\frac{\Delta E_L}{E_L}}_{from\ E_L} + \underbrace{\alpha \Delta T_O}_{from\ ocean}}^{water\ vapor\ supply} - \overbrace{\alpha \Delta T_L}^{warming} \Big) \tag{6}$$

$$\Delta RH_L = RH_L\Big(\overbrace{\alpha \Delta T_O}^{\substack{water\ vapor\ supply \\ from\ ocean}} - \overbrace{\alpha \Delta T_L}^{warming} \Big) \tag{7}$$

Eq. 6 describes changes in RH_L according to the proposed theory, while Eq. 7 describes changes in RH_L according to the ocean-influence theory. The sole disparity between the two equations lies in the initial term of Eq. 6, which represents the water vapor supply from E_L. RH_L can decline if the increase in water vapor supply is slower than the increase in saturation vapour pressure resulting from atmospheric warming. On the other hand, RH_L may remain steady if the water vapor supply is sufficiently large to offset the warming effect of increasing atmospheric moisture storage capacity due to the Clausius-Clapeyron relation. Therefore, decomposing ΔRH_L into three components using Eq. 6 can help identify the primary sources of the difference between reanalysis and CMIP6 climate models.

Fig. 6 presents the results of applying Eqs. 6 and 7 to the two reanalysis datasets and CMIP6 GCMs. The first column shows that the decline in RH_L is underestimated in CMIP6 models compared to ERA5 and JRA-3Q. The second column demonstrates that Eq. 6 can reasonably replicate this difference in terms of the ensemble median ΔRH_L, although CMIP6 models exhibit more variability. If we omit the first term of Eq. 6 as implied in Eq. 7, ΔRH_L from CMIP6 aligns closely with reanalysis (third column of Fig. 6). This result suggests that the difference in ΔE_L between CMIP6 and reanalysis is a significant contributor to the ΔRH_L bias.

Specifically, we found that the difference in water vapor supply from E_L between reanalysis and CMIP6 is sufficient to account for the difference in ΔRH_L between the two. The ocean advection term is also higher in CMIP6 than in reanalysis, but this effect roughly cancels out as terrestrial warming is also higher in CMIP6 than in reanalysis. This implies that the larger ocean warming in CMIP6 compared to observations in the recent decade cannot entirely explain the ΔRH_L bias in CMIP6 because the amplified terrestrial warming is also higher in CMIP6. This result aligns with recent studies[35,47], which demonstrated that climate models prescribing observed ocean warming cannot completely resolve the ΔRH_L bias issue.

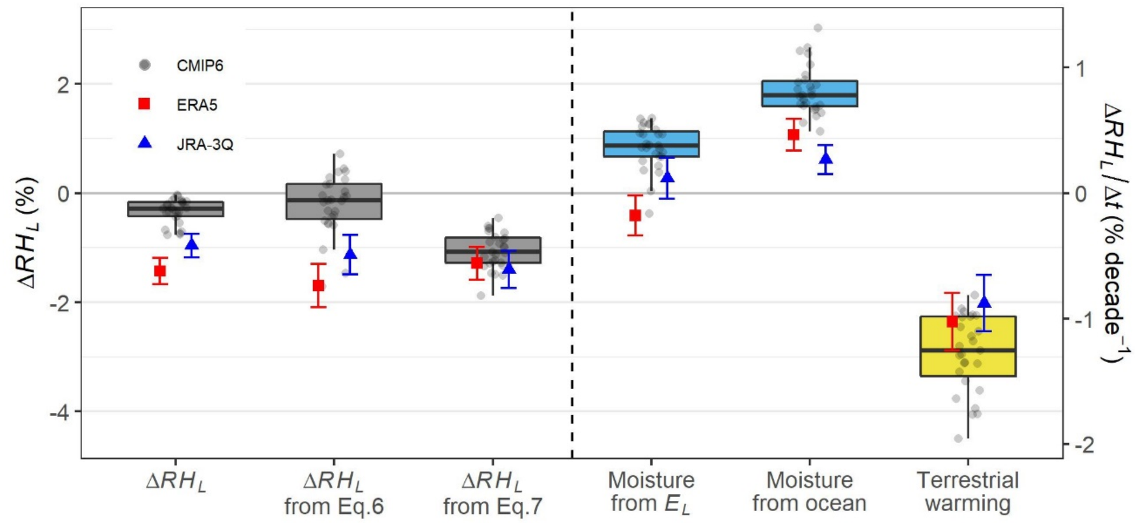

Fig. 6. Attribution of *ΔRH_L* based on Eq. 6. Box plots with jitter points depict CMIP6 models, while the red squares with error bars represent ERA5, and the blue triangles with error bars represent JRA-3Q. The first column is ΔRH_L, the second column is the estimated ΔRH_L using Eq. 6, and the third column is the estimated ΔRH_L using Eq. 7. The last three columns provide a breakdown of each term in Eq. 6. Here Δ indicates difference between current (2003-2022) and past climate (1980-1999). Error bars represent the 95% confidence intervals, and the secondary y-axis shows the average rate of change.

Discussion

Byrne and O'Gorman [27] demonstrated that a simple ocean advection constraint, as summarized in Eq. 1, along with another constraint on moist static enthalpy, can explain the observed decline in RH_L over land. At first glance, this ocean-influence theory may seem to be in contradiction with our proposed theoretical framework. However, reconciliation between the two theoretical frameworks is possible if ΔE_L is close to zero in Eq. 5.

Indeed, our analysis reveals that there are no significant global land E_L trends in ERA5 and JRA-3Q reanalysis for the past 43 years, although ERA5 suggests a slightly negative trend and JRA-3Q suggests a slightly positive trend. These subtle global land E_L trends are effectively replicated by our theoretical model of Eq. 5 (Fig. 3). These results suggest that the conventional ocean-influence theory and the present work can both be compatible within ERA5 and JRA-3Q reanalysis, which is known to assimilate in situ humidity observations and thus accurately reproduce the observed declining trend of RH_L [34,35].

On the other hand, most CMIP6 GCMs estimate positive global land E_L trends for the past 43 years (Fig. 4). This suggests that the left-hand side of Eq. 5 is positive, implying $\frac{\Delta q_L}{q_L} > \frac{\Delta q_O}{q_O}$. In other words, if an increase in q_L is faster than the rate suggested by the ocean-influence theory, it could imply an intensification of global land E_L. Recently, Seltzer, et al. [44] found that the paleotemperature proxies suggested $\Delta q_L = 0.84\Delta q_O$, where 0.84 is approximately 10-20%

larger than recent observations of $\frac{q_L}{q_O}(= 0.72)$ at the global scale [27]. This suggests that changes in q_L are faster than the rate suggested by the ocean-influence theory at the last glacial maximum, and it could potentially signify changes in E_L within the context of Eq. 5. Consequently, our theoretical framework remains consistent with recent paleotemperature proxies as well.

Our analysis illustrated in Fig. 6 suggests a potential overestimation of the intensification of terrestrial E_L in climate simulations, leading to a bias in ΔRH_L. This interpretation aligns with findings from a recent study[37], which identified certain plausible climate models within CMIP6 that exhibit a drier ΔRH_L. Notably, these plausible models generally demonstrate a weaker increase in E_L compared to other models, supporting our interpretation. If the intensification of E_L is indeed exaggerated in current state-of-the-art climate models, and if future projections also suffer from the same issue, as indicated by Douville and Willett [37], several significant implications may arise.

Firstly, the anticipated reduction in future soil moisture could be more severe than currently predicted by most models included in CMIP6. This is consequential because soil moisture reduction serves as a primary driver of the limited increase in E_L, leading to a decline in RH_L in climate models[31,32]. Secondly, the future ratio between annual mean runoff and annual mean precipitation (i.e., runoff ratio) might be underestimated due to the overestimated E_L[37]. The underestimated runoff ratio could imply a miscalculation of extreme flood events in the future based on current climate model projections. Thirdly, in alignment with the concerns raised by a recent study[35], the danger of wildfires and heatwaves may be more severe than predicted based on current climate models. If future E_L is constrained ($\Delta E_L \approx 0$), while RH_L decreases and temperature increases, extremely dry and hot weather conditions could become even more severe[48]. These implications highlight the importance of accurately modeling terrestrial evapotranspiration for a comprehensive understanding of future climate-related risks.

Although our initial, simplified E-influence theory in Eq. 3, which ignores ocean advection, tends to overestimate the global trend of E_L (Figs. 3 and 4), it provides a clear upper limit for the increase in global E_L based on the observed humidity trend over land. Specifically, considering that the ERA5 and JRA-3Q reanalysis closely aligns with the current trend of RH observations compared to climate simulations, Eq. 3 calculated using reanalysis meteorological data in Fig. 3 (i.e., 4 ~ 6 mm y^{-1} $decade^{-1}$) could serve as an upper limit for the increase in global E_L over past decades. It is unlikely for the global E_L increase to surpass this limit unless specific humidity over the ocean decreases, a scenario deemed unrealistic under a warming climate[49,50].

This upper limit based on humidity observations holds significance due to the substantial uncertainty in estimating the long-term global trend of E_L[5,6]. While recent water balance E_L estimations suggest a slight decreasing E_L trend[51], numerous remote sensing-based E_L estimates, employing physical equations, exceed 4 ~ 6 mm y^{-1} $decade^{-1}$[5,6]. Physically based E_L estimates from remote sensing often heavily depend on increases in temperature and net radiation, with the decrease in RH_L rarely considered or treated as an increase in E_L based on the atmospheric evaporative demand concept. However, our theory and analysis consistently demonstrate that a decrease in RH_L over this decadal time scale should not be interpreted as an increase in E_L. Rather, the decrease in RH_L should be understood as a consequence of a smaller increase in E_L to the water vapour supply within a coupled atmospheric boundary layer. This discrepancy in perspective may contribute to biases in physically based E_L estimations.

In this study, we present simple theoretical frameworks based on meteorological information to elucidate the source variability in E_L for climate models vs. observational data and reanalysis products. We employed this approach to evaluate trends in atmospheric humidity and E_L over past decades, particularly on a global scale. While our theory aligns consistently with observations, reanalysis, and climate models, certain limitations should be acknowledged in our methodology.

Firstly, our simple physical model relies on several simplified assumptions. For instance, Eq. 3 neglects local horizontal moisture advection, which could be a significant factor. Although Eq. 5 is introduced to account for horizontal moisture advection, it is only plausible at a global spatial scale, and therefore, it cannot accurately represent horizontal moisture advection at local scale. Consequently, our approach is not suitable for assessing regional scale long-term changes in E_L. A future study could enhance the model's regional scale applicability by incorporating additional advection terms into Eq. 5 or 3, providing a more accurate representation of local advection processes to understand regional changes in E_L.

Secondly, our approach is an analytical model instead of a process-based model, and as such, it cannot explain why E_L remained steady in reanalysis and was overestimated in CMIP6 climate simulations. This discrepancy could be related to surface parameterizations, considering factors such as stomatal closure due to the CO_2 fertilization effect[47]. Soil moisture limitation on E is another potential mechanism[31,32]. To better grasp the origin of this issue, future studies may explore the relationship between satellite soil moisture, E_L, and atmospheric humidity. Also, it is important to conduct experiments using land surface models with varying parameters or model structures to better understand the origin of the bias.

Methods

FLUXNET2015 data

To assess the proposed Eq. 3, we used the FLUXNET2015 Tier One (CC-BY-4.0) dataset[38]. This global dataset includes 212 in-situ eddy-covariance flux tower sites around globe representing over 1,500 site years. Monthly records of latent heat flux, air temperature, vapor pressure deficit, and air pressure were obtained from the FLUXNET data portal (https://fluxnet.org/data/fluxnet2015-dataset/). We only included data for periods for which the quality control flag indicated more than 80% of the half-hourly data were used for generating the monthly datasets (i.e., measured data or good quality gap-filled data). Also, we only included data points with positive latent heat flux. Additionally, we considered only sites with at least three consecutive months of available data. Following these filtering processes, 170 flux sites around the globe were retained.

The calculation of E_L was derived from latent heat flux, α from temperature ($\alpha = \frac{s}{q^*(T)} = \frac{L_v}{R_v T^2}$, where L_v is latent heat of vaporization and R_v is the gas constant for water vapor), and RH from temperature, air pressure, and vapor pressure deficit using the bigleaf R package[52]. The multiplications of ΔRH_L and ΔT_L in Eq. 3 were averaged values over the two months, with ΔRH_L and ΔT_L calculated as the difference between the two months. In Fig. 2, observed latent heat flux, without energy balance correction, was employed. Notably, we found similar results when using the energy balance correction version of latent heat flux, incorporating the Bowen ratio preservation method[38,53] (see Fig. S2).

ERA5 and JRA-3Q reanalysis

To evaluate the proposed theoretical framework, we employed ERA5, the latest reanalysis product from the European Center for Medium Range Weather Forecasts (ECMWF)[39], and JRA-3Q, the latest reanalysis product from the Japan Meteorological Agency[40]. It is worth noting that, in this study, we deliberately excluded MERRA2 reanalysis, another widely used reanalysis product by the National Aeronautics and Space Administration (NASA). This decision was based on MERRA2's limitation of not assimilating in situ humidity observations and its documented tendency to overestimate specific humidity trends[35].

We obtained ERA5 single level (near-surface) output from the Climate Data Store (CDS) of ECMWF (https://doi.org/10.24381/cds.f17050d7), and JRA-3Q single level (near-surface: 2 m height) output at 1.25 degree spatial resolution from the Data Integration and Analysis System (DIAS) (https://doi.org/10.20783/DIAS.645). We obtained monthly records of latent heat flux, air pressure, air temperature, and dewpoint temperature for the period of 1980-2022. We then calculated E from latent heat flux, α from temperature, and RH from temperature, air pressure, and dewpoint temperature using the bigleaf R package[52].

CMIP6 models

In addition to the two reanalysis datasets, we incorporated data from 27 climate models within the CMIP6[41]. The complete list of the utilized climate models is detailed in Table S1. For the analysis, we employed the Historical simulation covering the period from 1980 to 2014. Given that the historical simulation ended in 2014, we augmented our dataset with Shared Socioeconomic Pathway 5-8.5 (SSP5-8.5) simulations for the subsequent period from 2015 to 2022 to ensure comparability with the reanalysis datasets. We obtained monthly scale climate models' output from CDS of ECMWF (https://doi.org/10.24381/cds.c866074c). Latent heat flux, near-surface air temperature, near-surface air specific humidity, and surface air pressure were retrieved. We then calculated E from latent heat flux, α from temperature, and RH from temperature, air pressure, and specific humidity.

Derivation of the *E*-influence theory

Byrne and O'Gorman [26] introduced an idealized atmospheric boundary layer (ABL) box model to elucidate the relationship among horizontal moisture advection from the ocean, terrestrial E_L, and the vertical relaxation flux of moisture at the top of the ABL (e.g., entrainment). This idealized box model assumes a fixed ABL height and can be conceptualized as a diel-averaged ABL, similar to another ABL box model introduced elsewhere[16,18]. The moisture budget within the ABL box over land can be expressed as follows (Fig. S1):

$$h_L \frac{dq_L}{dt} = \frac{h_O}{l} \rho v_1 (q_O - q_L) + \frac{h_L - h_O}{l} \rho v_1 \left(q_{FT,O} - q_L\right) + \rho v_2 \left(q_{FT,L} - q_L\right) + E_L \tag{8}$$

where h is the boundary layer height, l is the length of the land, q is specific humidity, v_1 is horizontal mixing velocity, v_2 is vertical mixing velocity, and ρ is the air density. The subscripts O and L respectively denote ocean and land, while the subscript FT indicates the free troposphere immediately above the land and ocean boundary layers. Under steady-state conditions, the right-hand side is set to zero (i.e., $\frac{dq_L}{dt} = 0$). Byrne and O'Gorman [26] further simplified Eq. 8 by assuming that the free-tropospheric specific humidity is directly proportional to the ABL specific humidity, denoted as $q_{FT,L} = \lambda_L q_L$ and $q_{FT,O} = \lambda_O q_O$, where λ_L and λ_O are time constants. This assumption is also consistent with another derivation of the ocean-influence theory based on Lagrangian path-integral [25], where they assumed λ_L to be zero.

While the prior study focused on the horizontal advection from the ocean by assuming negligible E_L, we assume negligible horizontal advection. This assumption is justifiable in inland regions where horizontal specific humidity differences are minimal (see Fig. 1). Mathematically, the assumption of negligible horizontal advection can be expressed by considering $l \to \infty$ in Eq. 8, resulting in the following expression:

$$q_L = \frac{1}{\rho v_2 (1 - \lambda_L)} E_L \tag{9}$$

or

$$q_L = \beta E_L \tag{10}$$

where $\beta = 1/\rho v_2 (1 - \lambda_L)$, which depends primarily on the vertical mixing velocity at the top of the ABL. At a climatically-relevant time scale and a global spatial scale, β could be considered time constant because (1) changes in v_2 can be damped by multiplication by $1 - \lambda_L$, and (2) consistent changes in v_2 across all land grid are unrealistic, although significant local-scale changes in v_2 could occur [25]. If we assume β as time constant, β can be understood as a partial derivative of q_L with respect to E. The constant β in Eq. 10 also implies that the ratio of q_L and E_L remains approximately constant. Therefore, we can write as follows:

$$\frac{\partial q_L}{\partial E_L} = \beta \tag{11}$$

and

$$\frac{\Delta q_L}{q_L} = \frac{\Delta E_L}{E_L} \tag{12}$$

It is worth noting that Eq. 11 is conceptually similar to the sensitivity of the specific humidity to changes in E introduced by McColl, et al. [16]. In their work, they also showed that $\frac{\partial q_L}{\partial E}$ is largely governed by the vertical mixing velocity at the top of ABL (i.e., the relaxation conductance in their notation).

Eq. 12 leads to Eq. 2 in the main text.

Application of the proposed equations to reanalysis and GCMs

The proposed Eq. 3 was applied to each land grid cell. Specifically, we first calculated the climatology of the multiplications of ΔRH_L and ΔT_L in Eq. 3 for each month and grid. For the reanalysis applications presented in Fig. 3, the monthly climatology was multiplied by monthly anomalies of RH_L and T_L at each grid cell. The resulting values for each grid cell and month were spatially averaged with cosine-latitude weighting before computing annual average. In the case of CMIP6 climate models depicted in Fig. 4, the monthly climatology was multiplied by ΔRH_L and ΔT_L representing the difference between the current (2003-2022) and past (1980-1999) climate. Similar to the reanalysis dataset, the products were then spatially averaged using cosine-latitude weighting.

The application of Eq. 5 paralleled that of Eq. 3, with the distinction that the ocean temperature term (ΔT_O) needed to be incorporated. ΔT_O was individually computed for each ocean grid cell and subsequently spatially averaged using cosine-latitude weighting to derive the global average. These global averaged ΔT_O values were then introduced to each land grid cell for the application of Eq. 5. The computation of other variables in Eq. 5 followed the same methodology as outlined for Eq. 3.

In generating Fig. 6, which shows the application results of Eqs. 6 and 7, a challenge arose when attempting to apply the equation to each grid cell. This challenge was rooted in the fact that the first term on the right-hand side of Eq. 6 increases infinitely when E_L approaches zero. To address this issue, $\frac{RH_L}{E_L}$ was computed as the global mean of RH_L divided by the global mean of E_L. Subsequently, this global $\frac{RH_L}{E_L}$ value was multiplied to Eq. 5 to derive Eq. 6, while other variables were calculated at each grid cell and then spatially averaged by following the same methodology as outlined in the above paragraph.

Data availability

All data used in the main text and the supplementary information are publicly available. The FLUXNET2015 dataset can be obtained from the FLUXNET data portal (https://fluxnet.org/data/fluxnet2015-dataset/), the ERA5 reanalysis data can be obtained from CDS of ECMWF (https://doi.org/10.24381/cds.f17050d7), the JRA-3Q reanalysis data can be obtained from DIAS (https://doi.org/10.20783/DIAS.645), the CMIP6 models outputs can be obtained from CDS of the ECMWF (https://doi.org/10.24381/cds.c866074c).

Code availability

The code used for these analyses will be publicly available prior to publication.

References

1 Milly, P. C. D. *et al.* Stationarity Is Dead: Whither Water Management? *Science* **319**, 573-574, (2008).

2 Jung, M. *et al.* Recent decline in the global land evapotranspiration trend due to limited moisture supply. *Nature* **467**, 951-954, (2010).

3 Fisher, J. B. *et al.* The future of evapotranspiration: Global requirements for ecosystem functioning, carbon and climate feedbacks, agricultural management, and water resources. *Water Resour. Res.* **53**, 2618-2626, (2017).

4 Milly, P. C. D. & Dunne, K. A. Colorado River flow dwindles as warming-driven loss of reflective snow energizes evaporation. *Science* **367**, 1252-1255, (2020).

5 Pan, S. *et al.* Evaluation of global terrestrial evapotranspiration using state-of-the-art approaches in remote sensing, machine learning and land surface modeling. *Hydrol. Earth Syst. Sci.* **24**, 1485-1509, (2020).

6 Yang, Y. *et al.* Evapotranspiration on a greening Earth. *Nat. Rev. Earth Environ.* **4**, 626-641, (2023).

7 Sherwood, S. & Fu, Q. A drier future? *Science* **343**, 737-739, (2014).

8 Vicente-Serrano, S. M., McVicar, T. R., Miralles, D. G., Yang, Y. & Tomas-Burguera, M. Unraveling the influence of atmospheric evaporative demand on drought and its response to climate change. *WIREs Clim. Chang.* **11**, e632, (2020).

9 McColl, K. A., Roderick, M. L., Berg, A. & Scheff, J. The terrestrial water cycle in a warming world. *Nat. Clim. Chang.* **12**, 604-606, (2022).

10 Scheff, J., Coats, S. & Laguë, M. M. Why do the Global Warming Responses of Land-Surface Models and Climatic Dryness Metrics Disagree? *Earth's Future* **10**, e2022EF002814, (2022).

11 Ault, T. R. On the essentials of drought in a changing climate. *Science* **368**, 256-260, (2020).

12 Wang, L. *et al.* Dryland productivity under a changing climate. *Nat. Clim. Chang.* **12**, 981-994, (2022).

13 Zaitchik, B. F., Rodell, M., Biasutti, M. & Seneviratne, S. I. Wetting and drying trends under climate change. *Nat. Water.* **1**, 502-513, (2023).

14 Milly, P. C. D. & Dunne, K. A. Potential evapotranspiration and continental drying. *Nat. Clim. Chang.* **6**, 946-949, (2016).

15 Gentine, P., Chhang, A., Rigden, A. & Salvucci, G. Evaporation estimates using weather station data and boundary layer theory. *Geophys. Res. Lett.* **43**, 11,661-611,670, (2016).

16 McColl, K. A., Salvucci, G. D. & Gentine, P. Surface flux equilibrium theory explains an empirical estimate of water-limited daily evapotranspiration. *J. Adv. Model. Earth Syst.* **11**, 2036-2049, (2019).

17 Kim, Y. *et al.* Relative humidity gradients as a key constraint on terrestrial water and energy fluxes. *Hydrol. Earth Syst. Sci.* **25**, 5175-5191, (2021).

18 Vargas Zeppetello, L. R. *et al.* Apparent surface conductance sensitivity to vapour pressure deficit in the absence of plants. *Nat. Water.* **1**, 941-951, (2023).

19 Kim, Y., Garcia, M., Black, T. A. & Johnson, M. Assessing the complementary role of surface flux equilibrium (SFE) theory and maximum entropy production (MEP) principle in the estimation of actual evapotranspiration. *J. Adv. Model. Earth Syst.* **15**, (2023).

20 McColl, K. A. & Tang, L. I. An Analytic Theory of Near-Surface Relative Humidity over Land. *J. Clim.* **37**, 1213-1230, (2024).

21 Ma, H.-Y. *et al.* CAUSES: On the Role of Surface Energy Budget Errors to the Warm Surface Air Temperature Error Over the Central United States. *J. Geophys. Res. Atmos.* **123**, 2888-2909, (2018).

22 Dong, J., Lei, F. & Crow, W. T. Land transpiration-evaporation partitioning errors responsible for modeled summertime warm bias in the central United States. *Nat. Commun* **13**, 336, (2022).

23 Willett, K. *et al.* HadISDH land surface multi-variable humidity and temperature record for climate monitoring. *Clim. Past* **10**, 1983–2006, (2014).

24 Simmons, A. J., Willett, K. M., Jones, P. D., Thorne, P. W. & Dee, D. P. Low-frequency variations in surface atmospheric humidity, temperature, and precipitation: Inferences from reanalyses and monthly gridded observational data sets. *J. Geophys. Res. Atmos.* **115**, (2010).

25 Chadwick, R., Good, P. & Willett, K. A Simple Moisture Advection Model of Specific Humidity Change over Land in Response to SST Warming. *J. Clim.* **29**, 7613-7632, (2016).

26 Byrne, M. P. & O'Gorman, P. A. Understanding decreases in land relative humidity with global warming: conceptual model and GCM simulations. *J. Clim.* **29**, 9045-9061, (2016).

27 Byrne, M. P. & O'Gorman, P. A. Trends in continental temperature and humidity directly linked to ocean warming. *Proc. Nat. Acad. Sci. U.S.A.* **115**, 4863-4868, (2018).

28 Berg, A. & Sheffield, J. Climate change and drought: the soil moisture perspective. *Curr. Clim. Change Rep.* **4**, 180-191, (2018).

29 Kim, Y., Garcia, M. & Johnson, M. Land-atmosphere coupling constrains increases to potential evaporation in a warming climate: Implications at local and global scales. *Earth's Future* **11**, e2022EF002886, (2023).

30 Vicente-Serrano, S. M. *et al.* Recent changes of relative humidity: regional connections with land and ocean processes. *Earth Syst. Dynam.* **9**, 915-937, (2018).

31 Berg, A. *et al.* Land–atmosphere feedbacks amplify aridity increase over land under global warming. *Nat. Clim. Chang.* **6**, 869-874, (2016).

32 Zhou, W., Leung, L. R. & Lu, J. The Role of Interactive Soil Moisture in Land Drying Under Anthropogenic Warming. *Geophys. Res. Lett.* **50**, e2023GL105308, (2023).

33 Douville, H. & Plazzotta, M. Midlatitude Summer Drying: An Underestimated Threat in CMIP5 Models? *Geophys. Res. Lett.* **44**, 9967-9975, (2017).

34 Dunn, R. J. H., Willett, K. M., Ciavarella, A. & Stott, P. A. Comparison of land surface humidity between observations and CMIP5 models. *Earth Syst. Dynam.* **8**, 719-747, (2017).

35 Simpson, I. R. *et al.* Observed humidity trends in dry regions contradict climate models. *Proc. Nat. Acad. Sci. U.S.A.* **121**, e2302480120, (2024).

36 Allan, R. P. *et al.* Advances in understanding large-scale responses of the water cycle to climate change. *Ann. N.Y. Acad. Sci.* **1472**, 49-75, (2020).

37 Douville, H. & Willett, K. M. A drier than expected future, supported by near-surface relative humidity observations. *Sci. Adv.* **9**, eade6253, (2023).

38 Pastorello, G. *et al.* The FLUXNET2015 dataset and the ONEFlux processing pipeline for eddy covariance data. *Sci. Data* **7**, 225, (2020).

39 Hersbach, H. *et al.* The ERA5 global reanalysis. *Q. J. Roy. Meteorol. Soc.* **146**, 1999-2049, (2020).

40 Kosaka, Y. *et al.* The JRA-3Q Reanalysis. *Journal of the Meteorological Society of Japan. Ser. II* **102**, 49-109, (2024).

41 Eyring, V. *et al.* Overview of the Coupled Model Intercomparison Project Phase 6 (CMIP6) experimental design and organization. *Geosci. Model Dev* **9**, 1937-1958, (2016).

42 McColl, K. A. & Rigden, A. J. Emergent Simplicity of Continental Evapotranspiration. *Geophys. Res. Lett.* **47**, e2020GL087101, (2020).

43 Chen, S., McColl, K. A., Berg, A. & Huang, Y. Surface Flux Equilibrium Estimates of Evapotranspiration at Large Spatial Scales. *J. Hydrometeorol.* **22**, 765-779, (2021).

44 Seltzer, A. M., Blard, P.-H., Sherwood, S. C. & Kageyama, M. Terrestrial amplification of past, present, and future climate change. *Sci. Adv.* **9**, eadf8119, (2023).

45 O'Gorman, P. A. & Muller, C. J. How closely do changes in surface and column water vapor follow Clausius–Clapeyron scaling in climate change simulations? *Environ. Res. Lett.* **5**, 025207, (2010).

46 Held, I. M. & Soden, B. J. Robust responses of the hydrological cycle to global warming. *J. Clim.* **19**, 5686-5699, (2006).

47 Douville, H. *et al.* Drivers of the enhanced decline of land near-surface relative humidity to abrupt 4xCO2 in CNRM-CM6-1. *Clim. Dyn.* **55**, 1613-1629, (2020).

48 Byrne, M. P. Amplified warming of extreme temperatures over tropical land. *Nat. Geosci.* **14**, 837-841, (2021).

49 Allan, R. P., Willett, K. M., John, V. O. & Trent, T. Global Changes in Water Vapor 1979–2020. *J. Geophys. Res. Atmos.* **127**, e2022JD036728, (2022).

50 Xu, W. *et al.* Weakened Increase in Global Near-Surface Water Vapor Pressure During the Last 20 Years. *Geophys. Res. Lett.* **51**, e2023GL107909, (2024).

51 Ma, N., Zhang, Y. & Szilagyi, J. Water-balance-based evapotranspiration for 56 large river basins: A benchmarking dataset for global terrestrial evapotranspiration modeling. *J. Hydrol.*, 130607, (2024).

52 Knauer, J., El-Madany, T. S., Zaehle, S. & Migliavacca, M. Bigleaf—An R package for the calculation of physical and physiological ecosystem properties from eddy covariance data. *PLOS ONE* **13**, e0201114, (2018).

53 Twine, T. E. *et al.* Correcting eddy-covariance flux underestimates over a grassland. *Agr. Forest Meteorol.* **103**, 279-300, (2000).

Acknowledgments

We acknowledge the support of the Canadian Space Agency (CSA) Grant 21SUESIELH. We are grateful for FLUXNET2015 site PIs, ERA5 and JRA-3Q reanalysis developing groups, and the CMIP6 climate modelling groups, and appreciate the efforts of data providers for producing and making available these datasets. We express our thanks to the development of the ocean-influence theory (by M. Byrne, P. O'Gorman, R. Chadwick, P. Good, K. Willett, and others) that inspired our theoretical framework.

Author contributions

Conceptualization: YK, MSJ
Methodology: YK, MSJ
Investigation: YK, MSJ
Visualization: YK
Supervision: MSJ
Writing—original draft: YK
Writing—review & editing: MSJ

Competing interests

Authors declare that they have no competing interests.

Supplementary Information

Supplementary Information file includes:
Figs. S1 to S2
Tables S1